STATE-THE-ART OF INVESTIGATIONS INTO THE FILAMENTATION OF HIGH-POWER SUBPICOSECOND LASER PULSES IN GASES

V.P. Kandidov, O.G. Kosareva, A. Broder, and S.L. Chin

Department of Physics, M.V. Lomonosov State University, Moscow
Department of Physics, Laval' University, Quebec, Canada
Received July 21, 1997

We demonstrate how to modify the model of the moving foci, developed for condensed media for explanation of experiments on filamentation of the high-power subpicosecond laser pulses in air. This modified model allows one to consider the gas ionization in the high-intensity laser field. The numerical simulation based on this model allows us to explain not only the filamentation phenomenon, but also the accompanying effects such as refocusing and the conical emission.

1. INTRODUCTION

The high-power subpicosecond lasers that become available recently make it possible to carry out investigations of filamentation of the supernarrow pulses in gas media. In experiments, Refs. 1–3, the filaments with the length of tens of meters were observed at propagation, in air, of the pulses of 150-230 fs with the peak power 5–50 GW at wavelengths equal to 775, Ref. 1, or 800 nm, Refs. 2 and 3. In these experiments the self-action of laser radiation was developed in conditions, which were not achievable earlier in the nonlinear atmospheric optics, Ref. 4. The diagram in Fig. 1 shows the power threshold of the main nonlinear-optical effects in the atmosphere versus time of the radiation propagation through the medium, Ref. 5. This diagram corresponds to the CO_2-laser beams propagating along the near ground paths. One can see, that for micro– and millisecond pulses the Kerr effect, which is the determining factor in the process of beam filamentation, is suppressed by other nonlinear effects with the lower power thresholds. In the picosecond range the self-focusing of the laser beam of Kerr type becomes a real fact in the atmosphere. The peak power P of the self-focusing in the air ($P_{\text{peak}}^{\text{theor}} = \frac{l^2}{2pn_2}$, Ref. 6, $n_2 \approx 5.6 \cdot 10^{-19}$ cm^2/W, according to Ref. 7) at $\lambda = 0.8$ μm is about two orders lower than at $\lambda = 10.6$ μm and it is approximately equal to $2 \cdot 10^9$ W, according to the theoretical calculations, and $P_{\text{peak}}^{\text{expt}} \approx 6 \cdot 10^9$ W, according to the experimental data, Ref. 3.

In this paper we overview modern concepts concerning the filamentation of high-power supernarrow laser pulses in air under conditions of ionization of the gas component in high-intensity light field. We explain the refocusing and the conical emission effects, accompanying the filamentation of laser pulses.

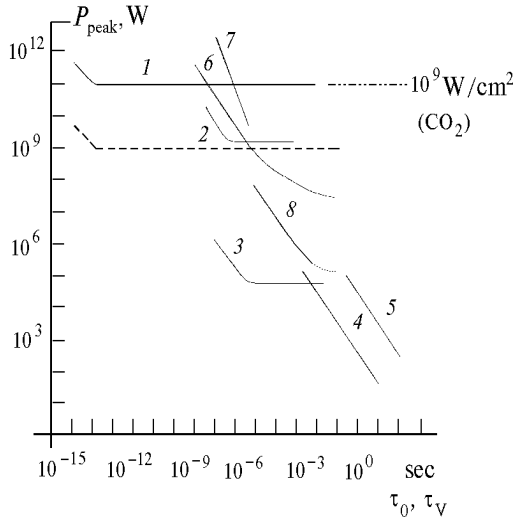

FIG. 1. The critical power level P_{peak} for some nonlinear optical effects in the atmosphere versus time of the beam propagation through the medium: the pulse duration τ_0 or the time of the wind refraction τ_V. Radius of the CO_2-laser beam is $a = 10$ cm, the molecular absorption $\alpha_m = 2 \cdot 10^{-4}$ m^{-1}, the wind speed $V = 10$ m/s; 1 is the Kerr effect; 2 is the electrostriction; 3 is the refraction on a sound wave; 4 is the wind refraction; 5 is the clearing up of a moving cloud; 6 is the optical breakdown on aerosol; 7 is the optical breakdown in the clear air; 8 is the kinetic cooling, dot-and-dash line shows the intensity of effect 1. Dashed curve denotes the P_{peak} for Kerr effect at $\lambda = 0.8$ μm.

2. FROM FILAMENTATION IN CONDENSED MEDIA TO THE FILAMENTATION IN GASES

First publications on investigations into the filamentation of high-power laser radiation in condensed media appeared more than thirty years ago.

0235-6880/97/12 966-08 $02.00

The history of the studies of this phenomenon is a good example of the evolution of physical conceptions in nonlinear optics. Experimental results on self-focusing of laser beams in a glass[8] and liquids[9] were qualitatively estimated by Chiao and co-authors,[10] and Garmire has measured the peak power threshold of the self-focusing in a chamber with CS_2, Ref. 11. First explanations of the filaments observed were associated with the self-contraction of high-power laser beam in a nonlinear medium. The stationary self-contraction of the beam in a medium with the Kerr nonlinearity was calculated theoretically by Talanov[12] and Kelley.[13]

Large contribution to the development of the theory of self-action of laser beams was introduced by Khochlov and his co-workers.[14] They constructed an analytical theory, describing the self-contraction of a laser beam in a nonaberration approximation. This theory covered the cases stationary self-focusing in a medium with an instant nonlinear response, and a nonstationary one in the media with the relaxation of Kerr and thermal nonlinearities. In the nonstationary case the nonlinearity is accumulated during a pulse, so that conditions of propagation of the pulse tail and its leading edge are essentially different.

The idea of moving foci applied to explanation of the filamentation of pulsed radiation was stated and advanced in Refs. 6, 15–17. According to the model of moving foci[6] the filament is a result of sequential change in the position of the self-focusing areas of various temporary layers of the pulse, the power in which varies with the changes in its shape. In Ref. 15 the nonlinear focusing of various ring-shaped areas in cross-section of the beam is considered to explain the occurrence of filaments at propagation of powerful pulses in optical materials. This model also included the effects of radiation saturation in a nonlinear focus, caused by two-photon absorption and stimulated Raman scattering (SRS). The experiments with the moving foci were documented for the first time in Refs. 16 and 17.

The self-focusing and filamentation of short laser pulses in a liquid with the relaxation nonlinearity of Kerr type were numerically calculated in Refs. 18 and 19.

The first explanation of the experiments on filamentation of subpicosecond laser pulses in air were associated, as earlier in the case of condensed media, with the self-contraction of radiation. According to Ref. 1 the Kerr nonlinearity stabilizes the diffraction divergence and defocusing in plasma, induced by the pulse due to ionization. In Ref. 2 the negative increment of the refractive index on a beam axis, caused by the self-induced plasma, forms the antiwaveguide, in which the steady flowing out modes are formed that are capable to propagate at large distances.

In Ref. 3 the filamentation of a laser pulse in air is explained by the model of moving foci, generalized on the case of gas media. In this model the gas ionization is essential when the intensity of the Kerr self-focusing reaches the ionization threshold. As a result the Kerr self-focusing on the leading edge of the pulse in air is replaced by the nonstationary plasma defocusing in the pulse tail.

3. EXPERIMENTS ON OBSERVING THE FILAMENTATION OF LASER PULSES IN AIR

The experiments discussed here used pulse-periodic radiation of a Titanium-Sapphire-based laser system. The arrangement of the experiments[3] is shown in Fig. 2. The central wavelength λ_0 is equal to 800 nm, the pulse duration is equal to 230 fs, the product $\Delta\nu\Delta t = 0.59$, the pulse repetition frequency is equal to 10 Hz. The beam radius at the intensity level of e^{-1} is equal to $a = (3.5 \pm 0.2)$ mm. The measurements were made for pulses of 2.3, 4.1, 6.1 and 8.1 mJ energy, that corresponded to the peak power of 9.4, 16, 25, and 33 GW. At the output from the optical compressor the pulse was delivered into a corridor with the help of two mirrors. The second mirror was located at a distance of 16.8 m from the output of the amplifier system. After this mirror the pulse freely propagated to the end of the corridor at the distance of 110 m. At the end of the path the energy decrease was equal to 20, 30, 35, and 40% of the initial energy 2.3, 4.1, 6.1, and 8.1 mJ, respectively.

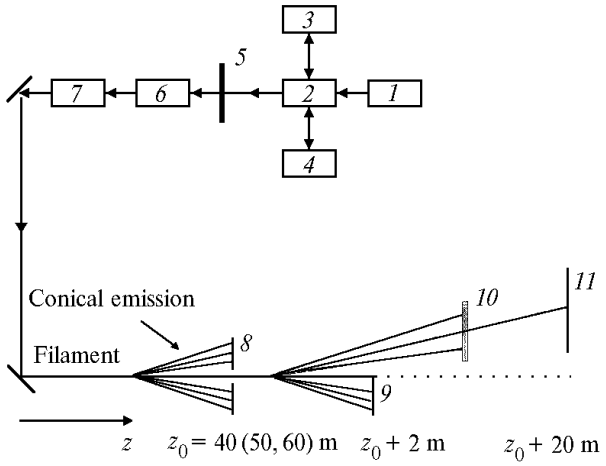

FIG. 2. The arrangement of experiments on observation of the laser pulse filamentation in air and of the conical emission: 1 is the master oscillator; 2 is the Faraday cell; 3 is the regenerative amplifier, 4 is the stretcher; 5 is the half-wave plate and polarizer for the control of pulse power; 6 is the Terawatt amplifier; 7 is the compressor; 8 is the round aperture of 4 mm *diameter; 9 is the blade; 10 is the interference filter; 11 is the screen.*

The initial qualitative observations of the pulse evolution were obtained with the help of photopaper. The beam images were recorded along the filament. At the distance from the output compressor of the laser system about 40 m the beam image on the photopaper was gradually compressed to a point at the center. At the distance of 40 m the beam image

was a grey circle with the diameter about 7 mm with the central black point about 1 mm in diameter. The pedestal, i.e., the grey circle in the beam image on the photopaper, is related to pulse layers which had not yet focused at the distance where the measurements were made. At the distance of 95 m the grey circle diameter decreased up to 2 mm, at the same time the central point has still been observed. The central point on the photopaper disappeared at the distance of 100 m, and that was considered as the filament length.

At the distance of 40 m and longer the conical emission was observed in the form of the concentric color rings, and the wavelength of radiation decreased with increasing radius of the ring. The ring with the largest radius corresponded to the wavelength of 500 nm.

To make the turbulence wandering of the beam lower, which were up to 3 mm at the end of the path, we created a closed channel from cardboard boxes for beam propagation. Thus, the characteristic scale of the natural atmospheric fluctuations was essentially decreased.

The quantitative information about the evolution of the beam was obtained with the help of measurement of total and axial energy, see Sec. 5, in this paper.

4. MOVING FOCI MODEL AT THE PRESENCE OF IONIZATION

In the process of beam self-focusing the intensity on its axis reaches 10^{14} W/cm^2. At this intensity the ionization of gas components appreciably influences pulse propagation in air, Ref. 20. The authors of experimental work[1] assumed the ionization to be the most probable mechanism, limiting the self-focusing, developed under conditions of pulse filamentation in air.

Contributions from the plasma and Kerr nonlinearities in the refractive index of air have opposite signs, and, at the first sight, one can expect, that these two mechanisms compensate each other at some intensity, providing the self-contraction. In reality, the situation is much more complex. The contribution coming from instantaneous Kerr nonlinearity increases and decreases proportionally to the pulse intensity, while the contribution from plasma nonlinearity is accumulated during the pulse. As a result the influence of the Kerr and plasma nonlinearities is different for different temporal parts of the pulse: the Kerr type of nonlinearity prevails in the leading edge of the pulse, while the plasma type of nonlinearity in the pulse tail. It is just that situation that explains the noninstantaneous response of a nonlinear medium. In the conditions considered the sophisticated treatment of spatiotemporal evolution of a pulse is possible by means of numerical simulations.

The propagation of a pulse in inert gases under the Kerr nonlinearity and ionization conditions was numerically considered earlier in Ref. 21 for the case of a focused beam and the peak power less then the peak value for self-focusing. Here we present some results of numerical simulations in conditions, typical for experiments on filamentation of high-power subpicosecond laser pulses in air,[3] where the initially collimated beam is used and its peak power exceeds the peak power of self-focusing.

The wave equation for pulse propagation is considered in the approximation of slowly varying amplitudes

$$2ik\left(\frac{\partial}{\partial z}+\frac{1}{v_g}\frac{\partial}{\partial t}\right)E=\Delta_\perp E+\frac{2k^2}{n_0}\Delta nE-ik\alpha E; \qquad (1)$$

$$\Delta n=\frac{1}{2}n_2|E|^2-\omega_p^2/(2\omega^2 n_0), \qquad (2)$$

where $\omega_p=\sqrt{4\pi e^2N_e/(m\omega^2)}$ is the plasma frequency and $n_0\approx 1$ in the air. The electron concentration N_e is calculated at each point of the space and time according to the equation for speed

$$\frac{\partial N_e}{\partial t}=R(N_0-N_e), \qquad (3)$$

where N_0 is the initial concentration of neutral molecules before the pulse. We consider the air to be a mix of nitrogen and oxygen. The most probable mechanism of the plasma formation up to the intensity of 10^{14} W/cm^2 at the wavelength equal to 800 nm is the multiphoton ionization of air components. In Eq. (3) R is the speed of the multiphoton ionization of oxygen (nitrogen), calculated according to the model from Ref. 22.

The factor $\alpha=I^{-1}l\hbar\omega(\partial N_e/\partial t)$ describes the energy losses due to generation of free electrons, where $I=\frac{cn_0}{8\pi}|E|^2$ is the intensity of the electrical field, and l is the order of the multiphoton process. Equation (1) does not take into account the dispersion of group speed of the pulse, as far as the dispersion blooming length for the pulse of 230 fs is about 800 m, that essentially exceeds the distances considered. In Eq. (3) the processes of shock ionization and recombination are not included, because their contribution into the considered pulse lengths is negligibly small.

In the experiment[3] the spatiotemporal distribution of intensity of the input pulse was close to the Gauss distribution. Therefore the initial field is taken in the form

$$E(r,\ z=0,\ \tau)=E_0\exp(-r^2/2a^2-\tau^2/2\tau_0^2), \qquad (4)$$

where $\tau=t-z/v_g$ is the time in the running system of coordinates; $\tau_0=138$ fs corresponds to the pulse duration of 230 fs, at half maximum level. At the numerical simulation the peak power P was taken to be $5\cdot P_{peak}^{theor}$. It corresponds to the peak power of 33 GW in experiment[3]: 33 GW $\approx 5\cdot P_{peak}^{expt}$, where $P_{peak}^{expt}=6$ GW.

The diameter of the input beam $a = 170$ μm was chosen to be less, than in the experiment ($a = 3.5$ mm) in order to be able to make calculations of both the initial and compressed beam on one and the same grid. Thus, the input peak intensity at the numerical simulation is $I_0 \approx 10^{13}$ W/cm^2, that exceeds the experimental one, which approximately equals to 10^{11} W/cm^2. Such an initial discrepancy does not influence qualitatively the pulse propagation since the ionization, which becomes essential at $I > 3 \cdot 10^{13}$ W/cm^2, occurs only in the vicinity of the nonlinear focus. For a comparison the results of numerical simulations and experimental data at the distance z are normalized to the corresponding diffraction length $z_d = \kappa a^2$, and the angle of conical emission θ_λ to the corresponding initial divergence $\theta_0 = \frac{\lambda_0}{2\pi a}$.

When $z_{sf} \approx 0.3\, z_d$, that corresponds to the nonlinear focus for the most powerful central layer ($\tau \approx 0$) of the pulse, the growth of the intensity I on the beam axis results in a fast increase of the electron concentration N_e. The influence of ionization extremely changes the evolution of the pulse. The distribution of intensity shows two main features, see Fig. 3, i.e., the unimodal structure of the beam on the leading edge of the pulse (Fig. 3*a*) and a ring structure in the cross-section of the beam at the pulse peak and tail (Fig. 3*b*).

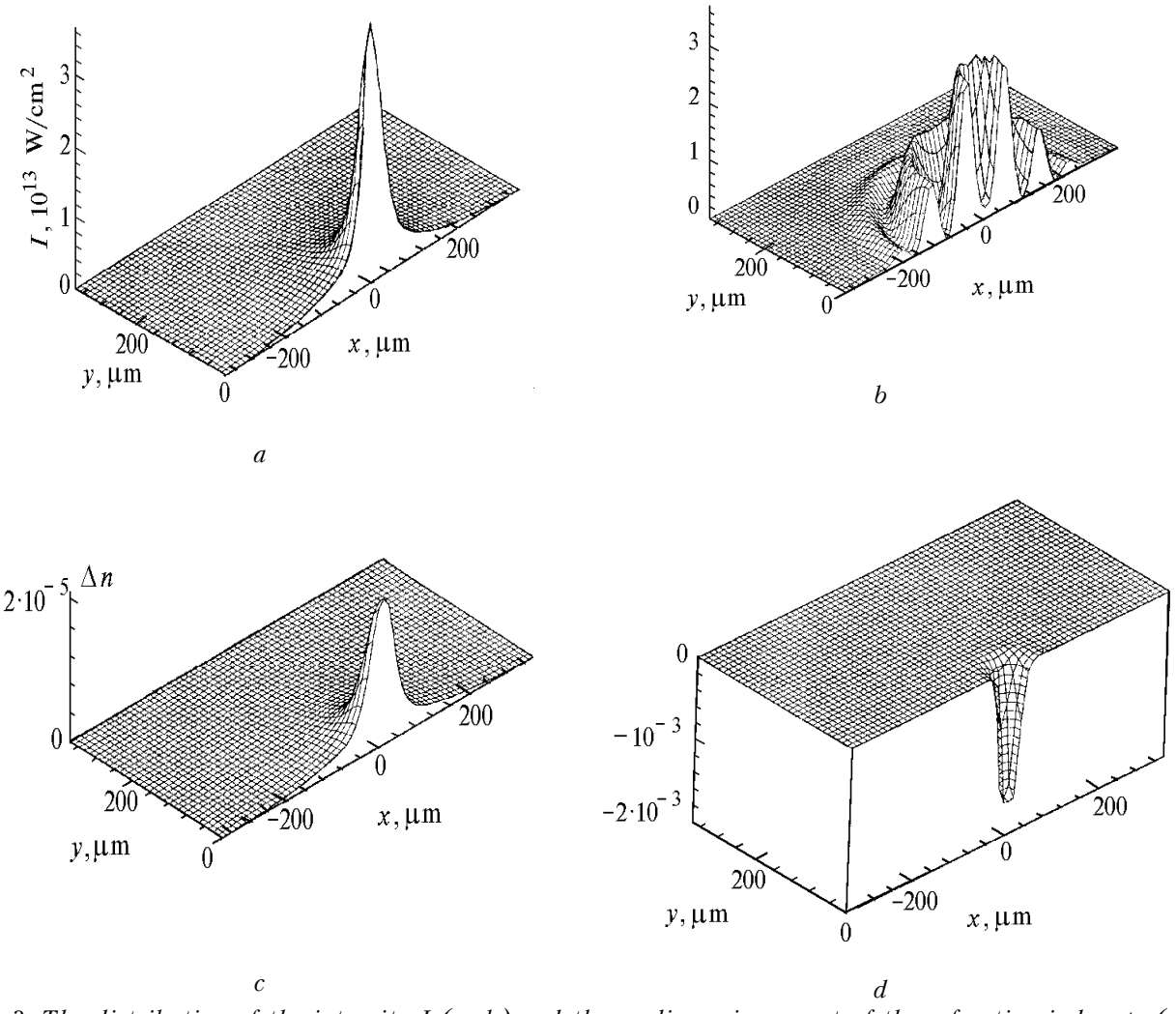

FIG. 3. The distribution of the intensity I (a, b) and the nonlinear increment of the refractive index Δn (c, d) in the cross-section of the beam at a distance $z = 0.34\, z_d$; $\tau = -116$ fs on the leading edge of the pulse (a, b); $\tau = 0$ at the pulse center (c, d).

Dynamics of each cross layer in the leading edge of the pulse can be characterized as a usual stationary self-focusing, since the concentration of electrons is negligibly small. Here the nonlinear addition to the refractive index Δn is determined by the Kerr nonlinearity and appears to be proportional to the intensity of radiation (cf. Fig. 3*a* and *b*). The evolution of the tail and central parts of the pulse (Fig. 3*b* and *d*) essentially differs from the evolution of the leading edge of the pulse. As

opposed to the Δn on the leading edge, the increment Δn at its center is negative and two orders higher in magnitude. It is because of a strongly nonlinear dependence of the speed of ionization R on the intensity I (about $R \propto I^8$). As a result, the plasma exerts the primary control over the propagation of the top and the tail of the pulse.

The spatiotemporal evolution of the pulse is shown in Fig. 4. The cross layers in the leading edge of the pulse are self-focused at the distances, corresponding to their power: the closer is the layer to the middle of the pulse, the shorter is the distance, at which this layer is focused (cf. Fig. 4*b*, *c*, and *d*). Thus, in accordance with the model of moving foci, the point of nonlinear focus for the leading edge of the pulse runs ahead in the direction of the radiation propagation, forming the filament observable in the experiment. On the pulse profile the focused layer is displaced ahead to its beginning.

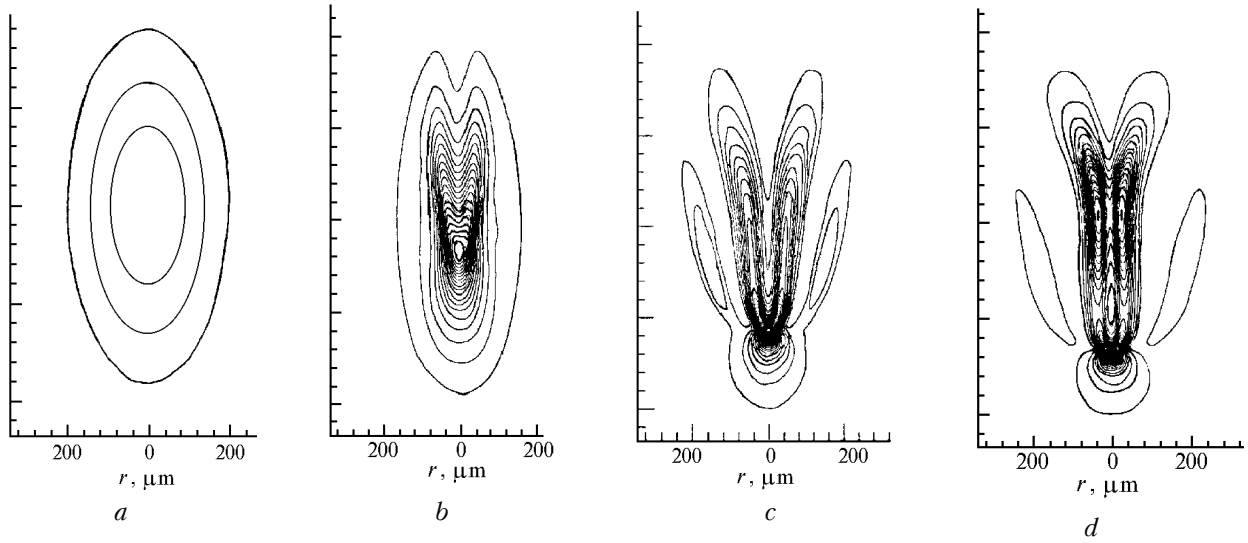

FIG. 4. Spatiotemporal evolution of the pulse in the filament; lines of equal intensity on the plane (r, τ): $z = 0$ (a), $0.28\, z_d$ (b), $0.34\, z_d$ (c), $0.42\, z_d$ (d). The intensity interval between contours is equal to $0.25 \cdot 10^{13}$ W/cm^2.

However the tail and the peak of a pulse do not follow the model of moving foci, developed for a condensed medium, Refs. 6, 15–17. The layers of these pulse parts dynamically defocuse in the self-induced plasma instead of self-focusing. That results in formation of rings in the cross-section of the beam. As a result, the spatiotemporal instability of radiation is developed at the pulse tail. The cause of the instability is the time delay of the nonlinear response of the medium under ionization conditions, i.e., the time dispersion of nonlinearity.[23]

The change of the coordinate z_{sf} of the moving focus versus time τ on the pulse profile is shown in Fig. 5. Curve *1*, obtained as a result of numerical simulation of the filamentation in conditions of ionization, shows the distance, at which the axial intensity reaches its maximum value, versus time τ. The branch of the curve *1* constructed for the leading edge of the pulse ($\tau < 0$) is close to the curve *2* corresponding to the classical model of moving foci, Ref. 6. The same branch of the curve *1*, constructed for the peak and the tail of the pulse, qualitatively differs from the curve *2*.

Since the cross distribution of the intensity in these parts of the pulse does not remain unimodal (Figs. 4*b–d*), then curve *1* in Fig. 5, for $\tau > -40$ fs, shows the distance, at which the given layer of the pulse decomposes into rings.

Thus, the classical model of moving foci in conditions of ionization is true only on the leading edge of the pulse in air, because the contribution of the plasma to the nonlinear part of the refractive index is so weak as to be negligible.

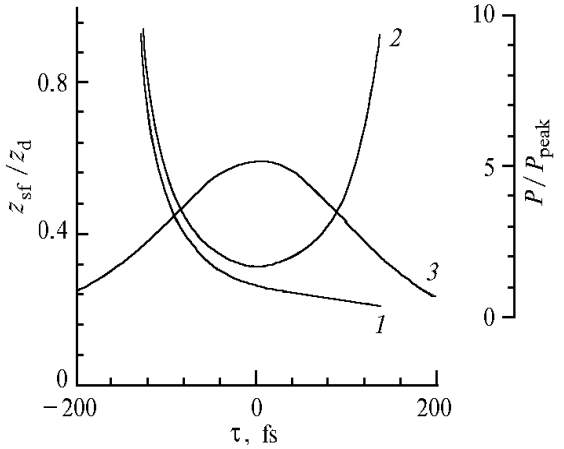

FIG. 5. Coordinate z_{sf} of the moving focus versus time τ on the pulse profile:1 is the model that accounts for the gas ionization; 2 is the model of moving foci for condensed media; 3 is the pulse shape.

5. REFOCUSING

The ionization of air in the process of filamentation results in the *refocusing* phenomenon, which was recorded experimentally by measurement of the filament power. The phenomenon of nonmonotonic change of the filament power versus distance was experimentally investigated in Ref. 3.

For the measure of the filament power, passing through the aperture with the center on the propagation axis, we took the power of the near axis part of the beam. The aperture diameter was equal to 500 μm, i.e., it was much less than the pedestal diameter (7 mm). It allowed us to monitor the change of the power in that cross-section of radiation, which forms the filament. The evolution of the radiation power $E_{\text{n.a.}}$, passed through the small aperture and normalized to the total pulse energy E_{T}, is shown in Fig. 6. The error of ± 5% lies within the limits of the symbol size in Fig. 6 and it is primarily due to fluctuations of the input pulse energy.

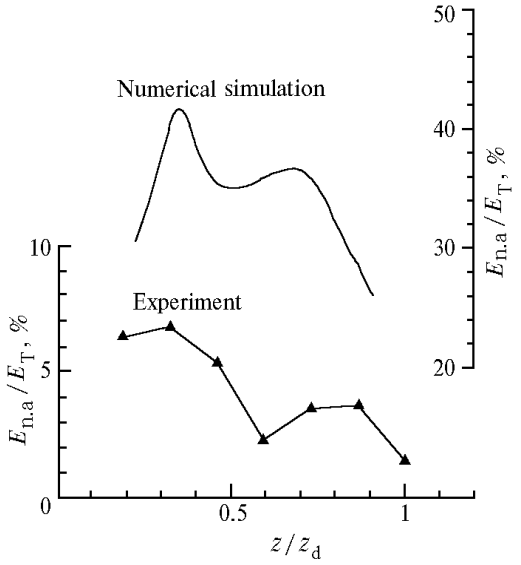

FIG. 6. The near axis pulse power (the filament power), normalized to the total pulse power versus distance z, normalized to the diffraction length z_{d}. The curve with closed triangles shows the experimental data (the left-hand vertical axis). The solid curve shows the results of numerical simulations (the right-hand vertical axis).

It is important to note the fact, that at any distance z the filament power, i.e., the radiation power, concentrated near the axis of propagation, was less than 7% of the total pulse energy at this z. It corresponds to the model of moving foci, according to which only a small part of the pulse layers is compressed in the vicinity of a given point z.

The computational near axis energy $E_{\text{n.a.}}^{\text{sim}}$, is determined as the energy, passed through the aperture with the diameter of 167 μm. Such an aperture size corresponds to the cross size of rings in the pulse tail, Fig. 4*d*, that allows to record its changes. It is necessary to notice, that in the numerical simulation the normalized energy, concentrated in the near axis area, is greater than that in real experiment, owing to the greater value of the ratio of the aperture diameter to the input beam diameter.

The results of numerical simulations are in a good qualitative agreement with the experimental data. The distance, at which the experimental and computational filament power reaches the first maximal value, coincides with the self-focusing length $z_{\text{sf}} \approx 0.3\, z_{\text{d}}$ of the most powerful central pulse layer. The spatiotemporal distribution of the pulse intensity at this distance is shown in Fig. 4*b*. The minimum of the filament power is a consequence of the strong defocusing of the pulse tail, Fig. 4*c*. The compression of defocused rings, i.e., refocusing, that is the cause of the second maximum occurrence, is demonstrated in Fig. 4*d* as the filament power versus distance.

The compression of rings at the pulse tail occurs owing to the positive value Δn on the beam periphery. Really, the nonlinear addition to the refractive index Δn is negative only in the small near axis area of the beam (Fig. 3*d*), where the intensity exceeds the ionization threshold $3 \cdot 10^{13}$ W/cm^2 due to self-focusing. On the beam periphery the contribution of the Kerr nonlinearity turned out to be greater than the contribution from plasma nonlinearity, because the intensity value is insufficient for creating the appreciable electron concentration. By increasing the scale of the vertical axis (Fig. 3*d*), one can see the positive contribution Δn in the refractive index (Fig. 7). It results in compression of rings, i.e., to the beam refocusing.

Despite that the positive contribution of the Kerr nonlinearity in Δn on the beam periphery is two orders of magnitude smaller than the contribution from plasma nonlinearity, this contribution is sufficient for a compression the ring structure at the pulse tail formed in the beam cross-section.

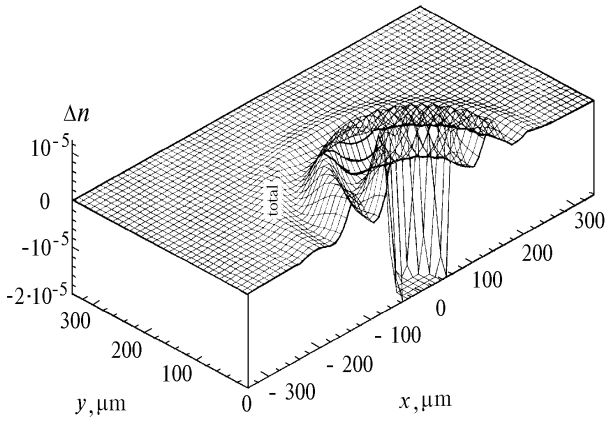

FIG. 7. Distribution of the nonlinear increment of the refractive index Δn, increased in comparison with Fig. 3d. The minimum in distribution cannot be seen on the scale used.

6. THE CONICAL EMISSION

The temporal changes of Δn, caused by the joint influence of the Kerr and plasma nonlinearities, induce a large spatiotemporal gradient of the electric field phase. This gradient, in turn, results in a strong transformation of the pulse spatiotemporal spectrum. The transformation of the spectrum is characterized by the occurrence of radiation, shifted to the short-wave region up to 500 nm. The angle of the pulse deviation from the propagation axis is larger at shorter wavelengths. In the far diffraction zone this pulse distribution looks as the conical emission, which was observed in filamentation conditions in air, Refs. 2 and 24, and numerically calculated in Ref. 24.

For the conical emission measurement the authors of experiment[24] placed a round aperture of 4 mm diameter at a given point z_0 on the filament propagation axis, and the blade, blocking the filament, at the point $z = z_0 + 2$ m, (Fig. 2).

Thus, the source of the conical emission was limited by the segment $z_0 < z < z_0 + 2$ m. The conical emission was recorded on a white screen, placed at the distance of 20 m after the aperture. The wavelength λ was selected by the interference filter with the resolution of 10 nm. The measurements of the radius of rings on the screen were made with the help of the ruler for $\lambda = 500$, 550, 600, and 650 nm and by the visualizer of IR–radiation for $\lambda = 700$ and 750 nm. The rings were not observed at the wavelength λ, greater than 800 nm. The conical emission angle θ_λ, owing to its small value, was determined as the ratio of the ring radius to the distance from the center of the conical emission source to the screen. The measurements were made for $z_0 \approx 40$, 50, and 60 m (0.42, 0.52, and 0.62 z_d, accordingly). The wavelength dependence of the angle θ_λ is shown by symbols in Fig. 8, where the angle value is specified both in degrees and in relative values, i.e., it is normalized to the initial divergence value of the beam $\theta_0 = \lambda_0/(2\pi a) = 0.0021°$.

In Fig. 8 one can see, that θ_λ does not depend on z_0. The vertical size of symbols corresponds to the measurement error, connected with the thickness of the ring, which is a consequence of the extension of the conical emission source and also of the limited value of the filter resolution.

For numerical simulations of the conical emission we have analyzed the frequency-angular distribution of the complex amplitude of the electrical field E. The wavelength dependences of the radiation propagation angle for the same filament points as in the experiment ($z = 0.42$, 0.52, and 0.62 z_d) are obtained (see Fig. 8, curves *1*, *2*, and *3*). The numerical and experimental dependences $\theta_\lambda(\lambda)$ qualitatively well agree and have the following characteristic features:

- the angle of the conical emission increases with decreasing wavelength from $\lambda_0 = 800$ nm to $\lambda \approx 500$ nm;
- the angle of the conical emission does not practically depend on the filament point;
- no conical emission occurs at $\lambda > 800$ nm.

The conical emission occurrence is connected with the phase self-modulation of the pulse in self-induced plasma. The pulse spectrum extension to the short-wave region, $\Delta\omega$, is expressed through the nonlinear shift of the phase $\varphi_{nl} = -\Delta n k z$ as $\Delta\omega = \partial\varphi_{nl}/\partial\tau \propto \partial N_e/\partial\tau$. The angular spectrum extension $k_\perp$ is proportional to the spatial derivative of the nonlinear phase shift $k_\perp = |\partial\varphi_{nl}/\partial r| \propto |\partial N_e/\partial r|$. In the self-focusing process there occurs simultaneously on the pulse front both strong spatial compression of the radiation in the radial direction, and the compression in time. It results in a fast and simultaneous spatiotemporal growth of the electron concentration N_e. As a result the radiation divergence $\theta_\lambda = k_\perp/k$ occurs to be larger the larger is the short-wave shift $\Delta\omega$. It is seen, that the angle of the conical emission strongly depends on the speed of the electron concentration growth.

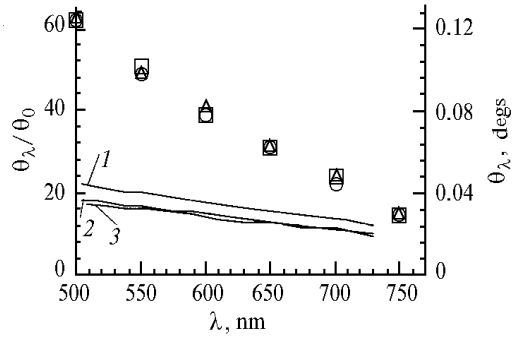

FIG. 8. The angle of the conical emission versus the wavelength of radiation, obtained in the laboratory (symbols) and numerical (solid curves) experiments, Ref. 24. The triangles correspond to $z = 40$ m, open circles to $z = 50$ m, and open squares to $z = 60$ m. In the numerical experiment it corresponds to $z = 0.42\ z_d$ (curve 1), $0.52\ z_d$ (curve 2), and $0.62\ z_d$ (curve 3). The right-hand vertical axis shows the absolute value of the conical emission angle, obtained in the laboratory experiment.

The numerical analysis made shows that quantitatively the conical emission angle θ_λ can correctly be obtained using the ionization model with the ionization threshold about 2.5 times higher, than the threshold in the used model from Ref. 22. Such a correction of the threshold intensity is in accordance with the recently conducted experiment, Ref. 25, which has shown, that the ionization threshold of the oxygen molecule is about two times higher than in the model from Ref. 22, owing to the dissociated recombination.

The absence of the Stokes radiation in the conical emission can be explained by the fact that the plasma nonlinearity causes only the antistokes extension of the spectrum and radiation that experiences maximum

phase self-modulation is defocused. The Kerr nonlinearity causes both the Stokes and antistokes spectrum extension. The strongest spectrum shift is observed on the beam axis due to the positive contribution of Kerr nonlinearity in Δn, i.e., the radiation at maximum of the phase self-modulation, is focused. Hence, the Kerr nonlinearity, not accompanied by other effects, cannot be the cause of the conical emission.

7. CONCLUSION

The origin of filaments formed by powerful subpicosecond laser pulses in air is similar to the filaments observed in condensed media, Refs. 8–11, 16, and 17. That and other filaments represent a sequence of foci created by the different pulse layers.

The filamentation of the subpicosecond laser pulses in air and the accompanying processes are described within the framework of the moving foci model, modified by the presence of ionization. According to this model the moving focus exists only on the leading edge of the pulse, where the ionization has no time to be developed. The pulse tail decomposed into rings owing to the defocusing in the self-induced plasma. Nonmonotonic change of the experimentally measured energy of the pulse filament versus distance occurs due to refocusing of the pulse tail in the self-induced plasma. Thus, the refocusing is a dynamic process of divergence and the compression of rings in the pulse tail.

The conical emission accompanying the filamentation of the subpicosecond pulse in air is the result of the phase self-modulation induced by the spatiotemporal nonlinearity of ionization. The laboratory experiment and the frequency-angular analysis of the electric field, obtained at the numerical simulation, have revealed the same typical features of the conical emission:

- the conical emission angle increases with decreasing wavelength from the initial at 800 nm to the green wavelength at 500 nm;
- the conical emission angles do not practically vary at the displacement of the measurement position along the filament;
- no conical emission occurs in the Stokes region of spectrum.

The analysis of nonstationary nonlinear interaction of the subpicosecond laser pulses with substance allows one to apply the model of moving foci to solving the problems of the optical destruction of materials by ultrashort pulses, the optical memory problems and so on.

REFERENCES

1. A. Braun, G. Korn, X. Liu, D. Du, J. Squier, and G. Mourou, Opt. Lett. **20**, 73 (1995).
2. E.T.J. Nibbering, P.F. Curley, G. Grillon, B.S. Prade, M.A. Franco, F. Salin, and A. Mysyrowicz, Opt. Lett. **21**, 62 (1996).
3. A. Brodeur, O.G. Kosareva, C.-Y. Chien, F.A. Ilkov, V.P. Kandidov, and S.L. Chin, Opt. Lett. **22**, 304 (1997).
4. V.E. Zuev, A.A. Zemlyanov, and Yu.D. Kopytin, *Nonlinear Atmospheric Optics* (Gidrometeoizdat, Leningrad, 1989), 256 pp.
5. V.P. Kandidov, in: *Nonlinear Optics and Optoacoustics of the Atmosphere* (Institute of Atmospheric Optics, Siberian Branch of the Academy of Sciences of the USSR, Tomsk, 1988), pp. 3–12.
6. J.H.Marburger, Prog. Kvant. Electron. **4**, 35 (1975).
7. Y. Shimoji, A.T. Fay, R.S.F. Chang, and N. Djeu, J. Opt. Soc. Am. **B6**, 1994 (1989).
8. M. Hercher, J. Opt. Soc. Am. **54**, 563 (1964).
9. N.F. Pilipetskii and A.R. Rustamov, Pis'ma Zh. Eksp. Teor. Fiz. **2**, 88–90 (1965).
10. R.Y. Chiao, E. Garmire, and C.H. Townes, Phys. Rev. Lett. **13**, 479–480 (1964).
11. E. Garmire, R.Y. Chiao, and C.H. Townes, Phys. Rev. Lett. **16**, 347 (1966).
12. V.I. Talanov, Pis'ma Zh. Eksp. Teor. Fiz. **2**, No. 5, 218–222 (1965).
13. P.L. Kelley, Phys. Rev. Lett. **15**, 1005–1008 (1965).
14. S.A. Akhmanov, A.P. Sukhorukov, and R.V. Khokhlov, Usp. Fiz. Nauk **93**, No. 1, 19–70 (1967).
15. V.N. Lugovoy and A.M. Prokhorov, Usp. Fiz. Nauk **111**, 203–247 (1973).
16. M.M.T. Loy and Y.R. Shen, Phys. Rev. Lett. **22**, 994 (1969).
17. V.V. Korobkin, A.P. Prokhorov, R.V. Serov, and M.Ya. Shchelev, Pis'ma Zh. Eksp. Teor. Fiz. **11**, 94 (1970).
18. J.A. Fleck, Jr., and P.L. Kelley, Appl. Phys. Lett. **13**, 313 (1969).
19. E. Shimizu, IBM J. Res. Dev. **17**, 286 (1972).
20. V.P. Kandidov, O.G. Kosareva, and S.A. Shlenov, Atmos. Oceanic Opt. **6**, No. 1, 48–52 (1993).
21. V.P. Kandidov, O.G. Kosareva, and S.A. Shlenov, Kvant. Elektron. **21**, 971–977 (1994).
22. A.D. Bandrauk, ed., *Atomic and Molecular Processes with Short Intense Laser Pulses* (Plenum Press, New York, 1987), 207 pp.
23. V.P. Kandidov, O.G. Kosareva, and S.A. Shlenov, Kvant. Elektron. **24**, 453–456 (1997).
24. O.G. Kosareva, A. Brodeur, C.-Y. Chien, V.P. Kandidov, and S.L. Chin, Opt. Lett. **22**, 1332–1334 (1997).
25. Talebpour, C.-Y. Chien, and S.L. Chin, J. Phys. **B**: Atomic and Molecular Physics **29**, L677 (1996).